AGU PUBLICATIONS

Geophysical Research Letters

RESEARCH LETTER
10.1002/2017GL074069

Key Points:
- We identify the first subsurface dome in the South Polar Layered Deposits using SHARAD data
- Calculations indicate that the dome is a physical structure that is offset to the east from Australe Mensa
- The location of the dome indicates the major H_2O snow/ice depositional center has recently oscillated in extent and location

Supporting Information:
- Supporting Information S1

Correspondence to:
J. L. Whitten,
whittenj@si.edu

Citation:
Whitten, J. L., B. A. Campbell, and G. A. Morgan (2017), A subsurface depocenter in the South Polar Layered Deposits of Mars, *Geophys. Res. Lett.*, *44*, 8188–8195, doi:10.1002/2017GL074069.

Received 5 MAY 2017
Accepted 7 AUG 2017
Accepted article online 10 AUG 2017
Published online 31 AUG 2017

A subsurface depocenter in the South Polar Layered Deposits of Mars

J. L. Whitten[1], B. A. Campbell[1], and G. A. Morgan[1]

[1]Smithsonian Institution, Washington, District of Columbia, USA

Abstract The South Polar Layered Deposits (SPLD) are one of the largest water ice reservoirs on Mars, and their accumulation is driven by variations in the climate primarily controlled by orbital forcings. Patterns of subsurface layering in the SPLD provide important information about past atmospheric dust content, periods of substantial erosion, and variations in local or regional deposition. Here we analyze the SPLD using SHAllow RADar (SHARAD) sounder data to gain a unique perspective on the interior structure of the deposits and to determine what subsurface layers indicate about the preserved climate history. SHARAD data reveal a major deviation from the gently domical layering typical of the SPLD: a subsurface elongate dome. The dome most likely formed due to variations in the accumulation of ice and snow across the cap, with a higher rate occurring in this region over a prolonged period. This SPLD depositional center provides an important marker of south polar climate patterns.

1. Introduction

The south polar region of Mars is covered with a deposit of layered H_2O ice, CO_2 ice, and dust known as the South Polar Layered Deposits (SPLD) (Figure 1). This layering is interpreted to record the climate history of Mars over at least the last 7–100 Myr (the SPLD surface has been dated to between 7.25 ± 3.6 and 14.5 ± 7.2 Ma [*Herkenhoff and Plaut*, 2000] and 30–100 Ma [*Koutnik et al.,* 2002]) and, as a result, images of the SPLD have been studied extensively [e.g., *Murray et al.,* 1972; *Howard et al.,* 1982; *Herkenhoff and Murray*, 1990; *Byrne and Ivanov*, 2004; *Milkovich and Plaut*, 2008]. Variations in the dust content of the subsurface layers may indicate changes in ice stability or dust loading. Correlations between orbital parameters such as obliquity, eccentricity, and precession, and layer structure and composition (e.g., H_2O ice versus CO_2 ice) may reveal the cause and effect relationship between these orbital parameters and the presence and morphologic characteristics of the polar layered deposits [*Murray et al.,* 1973; *Toon et al.,* 1980; *Thomas et al.,* 1992]. The SPLD is interpreted as almost entirely water ice [*Nye et al.,* 2000; *Titus et al.,* 2003; *Bibring et al.,* 2004; *Zuber et al.,* 2007; *Plaut et al.,* 2007], but the discovery of significant CO_2 reservoirs [*Phillips et al.,* 2011] has dramatic implications for paleo-atmospheric pressure regimes and the recent climate of Mars [e.g., *Bierson et al.,* 2016].

Several studies have analyzed the subsurface layering exposed in troughs and at the edge of the SPLD to characterize its overall internal structure. *Byrne and Ivanov* [2004] analyzed the elevation of outcrops in the top few hundred meters of the uppermost Bench Forming Layer (BFL) sequence to determine the overall shape of the SPLD subsurface layers. This layer sequence has a diagnostic pattern, including four morphologically distinct, bench-forming units. The locations of BFL outcrops indicate that the overall shape of the SPLD is a gently dipping dome with its apex in the center of Australe Mensa (86.88°S, 357.24°E). The dip angle of the layering suggests that the SPLD extent has not changed substantially from when the BFL sequence was emplaced. A later analysis of the SPLD internal structure by *Milkovich and Plaut* [2008] revealed three distinct layer sequences, from top to bottom: the Bench Forming Layer, Promethei Lingula Layer (PLL), and the Inferred Layer (IL). An outcrop of the lowermost IL sequence was only observed in one Thermal Emission Imaging System (THEMIS) visible image, but its regional extent was implied by elevation variations of the BFL and PLL sequences [*Byrne and Ivanov*, 2004; *Milkovich and Plaut*, 2008] not associated with basal topography [*Plaut et al.,* 2007]. This analysis of THEMIS image data confirmed previous results that the SPLD layers are dome shaped, but that the areal extent of each layer sequence differs; the BFL and IL more closely follow the current extent of the south pole residual cap (SPRC), compared with the PLL, which is found throughout the SPLD.

Previous studies relied on images of outcrops within troughs and at the edges of the SPLD. Radar sounder data provide a unique perspective, enabling a view into the subsurface to trace radar echoes from

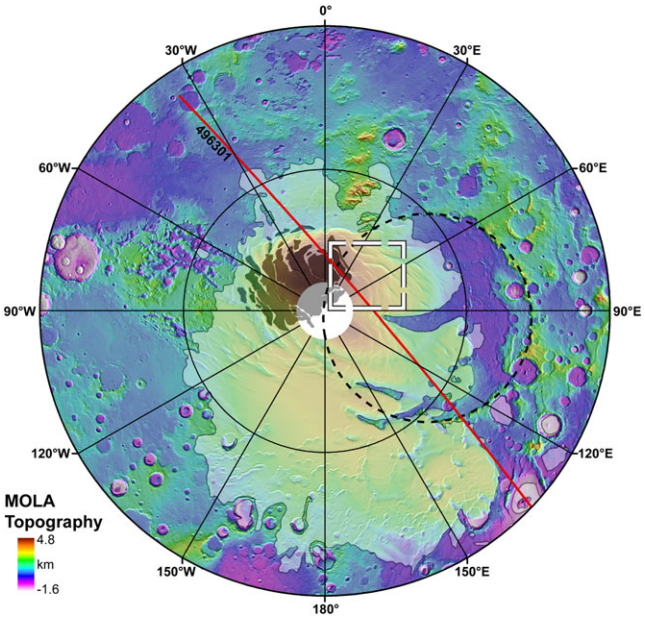

Figure 1. The South Polar Layered Deposits and the location of the subsurface elongate dome. The dome (white box) is identified in the SPLD (white tone overlay), just east of the residual ice cap (black tones). Red line denotes the location of SHARAD track 496301 (Figure 2). Dashed black circle is the rim of the Prometheus Basin (~875 km in diameter [*Condit and Soderblom*, 1978]). MOLA 128 ppd (~0.5 km/pixel) gridded topography [*Smith et al.,* 2001] over hillshade basemap.

reflecting interfaces throughout the deposit and produce reliable layer and sequence correlations [*Milkovich et al.,* 2009; *Christian et al.,* 2013]. Here we use data from the SHAllow RADar (SHARAD) on the Mars Reconnaissance Orbiter (MRO) to characterize the internal structure of the SPLD and to identify a feature very different from the simple view of a single regional domical layer structure. We then consider possible causes of this observed feature, including influences from basal topography, ice composition (H_2O versus CO_2), and snow/ice depositional centers.

2. Data and Methods

SHARAD sounder data are used to investigate the internal structure of the SPLD to better understand the unit depositional history. The SHARAD instrument aboard the MRO spacecraft has a 10 MHz bandwidth centered at 20 MHz [*Seu et al.,* 2004, 2007]. Measurements are displayed as radargrams, with time delay on the vertical axis and spacecraft position on the horizontal axis (Figure 2). After synthetic aperture processing the horizontal, or along-track, resolution is 0.3–1.0 km. The vertical resolution in free space is 15 m; in geologic materials the vertical range resolution improves, dependent upon the material dielectric properties. SHARAD has a vertical resolution of ~8.4 m in water ice with a dielectric constant (ε') of 3.15. Exposures of subsurface layers in troughs indicate that individual layers are on the order of 10 m thick and layer groups, or packets, are >100 m thick [*Byrne and Ivanov*, 2004; *Milkovich and Plaut*, 2008]. Thus, it is difficult to observe individual layers in SHARAD, but layer packets are resolvable.

In the SPLD, the radar signal is often attenuated to the point that it does not reveal some/all of the underlying interfaces (Figure S1 in the supporting information). In particular, the radar signal undergoes a diffuse

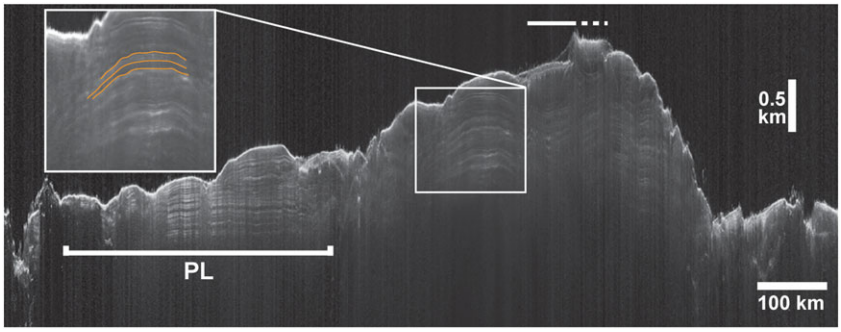

Figure 2. Radargram of a subsection of SHARAD track 496301. This water ice depth-corrected radargram was processed using the incoherent summing technique [*Campbell et al.,* 2015], which enhances subsurface layer visibility. Compare the shape of the layers that define the dome structure (inside white box) with the expected horizontal layering in Promethei Lingula (PL). The white horizontal bar above the SPLD indicates the approximate location of CO_2 ice [*Bierson et al.,* 2016]; solid white shows where CO_2 ice is mapped, and dashed white shows the location of off-nadir CO_2 ice that may influence the position of radar echoes. Orange lines in inset trace reflector boundaries and show variation in layer thickness.

backscattering process that causes a bright background echo known informally as "fog" [*Campbell et al.,* 2014, 2015]. *Campbell et al*. [2015] developed an incoherent summing technique to increase the signal-to-noise ratio of SHARAD radargrams available in the Planetary Data System in order to more readily trace subsurface radar echoes [*Campbell et al.,* 2015] (Figure S1). In this technique, radar echoes from tracks that overlap within 1 km of the ground point of a reference track are summed. The greatest improvement in the signal-to-noise ratio of the radargrams occurs in regions closest to the MRO coverage gap around the pole. In this study, 918 SHARAD radargrams were processed using this incoherent summing technique in order to map the extent of subsurface reflectors in the SPLD (Figure 2).

In order to evaluate the structure of the SPLD and trace internal layers, the radargrams were depth-corrected [e.g., *Putzig et al.,* 2009; *Phillips et al.,* 2011] using a real dielectric constant (ε') of 3.15 for the subsurface, a typical value of pure water ice under Martian conditions [*Johari*, 1976; *Grima et al.,* 2009]. It is plausible that another material, such as CO_2 ice, is present and contributing to the vertical position of the radar reflectors. For example, if a water ice depth correction was applied to a column of material with a substantial amount of CO_2, the subsurface layers are expected to deform upward due to the lower real dielectric constant for CO_2 (~2.1 [*Simpson et al.,* 1980; *Pettinelli et al.,* 2003]). Therefore, if the water ice depth correction produced non-horizontal surfaces in the radargrams analyzed, the amount of CO_2 and H_2O ice required to move the vertical position of a convex upward reflector into line with other horizontal reflectors was calculated.

3. Non-horizontal Layering in the SPLD

Analysis of 918 SHARAD radargrams corrected for the speed of light in H_2O ice indicates that substantial local variations in the layer structure of the SPLD occur to the east of Australe Mensa, just east of the SPRC. This structure, interpreted as an elongate dome, is evident in 381 radargrams (Figure S2 and Table S1). Most of the SPLD structure, identified by radar echoes interpreted to result from interfaces between ice layers and more concentrated dust layers, is near-horizontal. Close to this thickest part of the deposit, however, there is a region where the layering traces a convex upward or domical cross section (Figures 2 and 3). The radar interfaces exhibit a convex upward shape from the surface down to the last detectable reflector (Figure 2); the elongate dome is defined as the entire series of convex upward reflectors visible in the radargrams. In some radargrams the radar reflectors are visible for large horizontal distances, and in other SHARAD track orientations the series of reflectors composing the dome are visible for smaller horizontal distances. This positive relief feature is observed in single-track radargrams, but is most apparent in those processed using an incoherent summing technique to add echoes from overlapping tracks (Figure S1). There are other smaller, nonhorizontal features in the SPLD; here we focus on the largest detected.

The large convex upward structure has a maximum diameter of ~210 km, measured from its largest horizontal extent in the radargrams, and its crest, or highest point on the uppermost reflector, is ~200–300 m below the SPLD surface. The mean difference between a near-horizontal layer (e.g., Figure 4, right hand side of radargrams) and the dome crest is ~280 m (for a dielectric permittivity $\varepsilon' = 3.15$, consistent with H_2O ice [*Johari*, 1976; *Grima et al.,* 2009]) (Figure 3). The morphology of the structure changes with depth; it evolves from a double-crested feature to a single-crested feature with increased elevation (Figure 2), though the same sequence or spacing of the elongate dome radar reflectors is observed in all of the SHARAD radargrams. This change in morphology is most apparent in the southernmost SHARAD tracks, which are tangent to the polar coverage gap. There is no evidence for unconformities or layers pinching out near this positive relief feature. Several of the structure-tracing layers continue hundreds of kilometers across the SPLD, from the side of the structure downward into regions of near-horizontal layering (Figure 4). In cross section, the subsurface layers along the domical structure subtly change in thickness, being thickest toward the crest of the feature and thinning downslope as the radar reflectors approach horizontal (Figures 2 and 3). Measurements of radar time delay indicate that the layers can be up to 20 m thicker at the crest compared with the descending slopes of the convex upward structure (Figure 2, orange lines).

When viewed together, all of the identified positive relief features traced in cross section form a 3-D elongate dome structure (Figure 3), centered at approximately 87.0°S 49.3°E. The center of the elongate dome may be even closer to the geographic south pole, but due to the polar coverage gap resulting from the MRO orbit inclination, it is difficult to precisely measure the southern extent of the feature. Integrating from the base

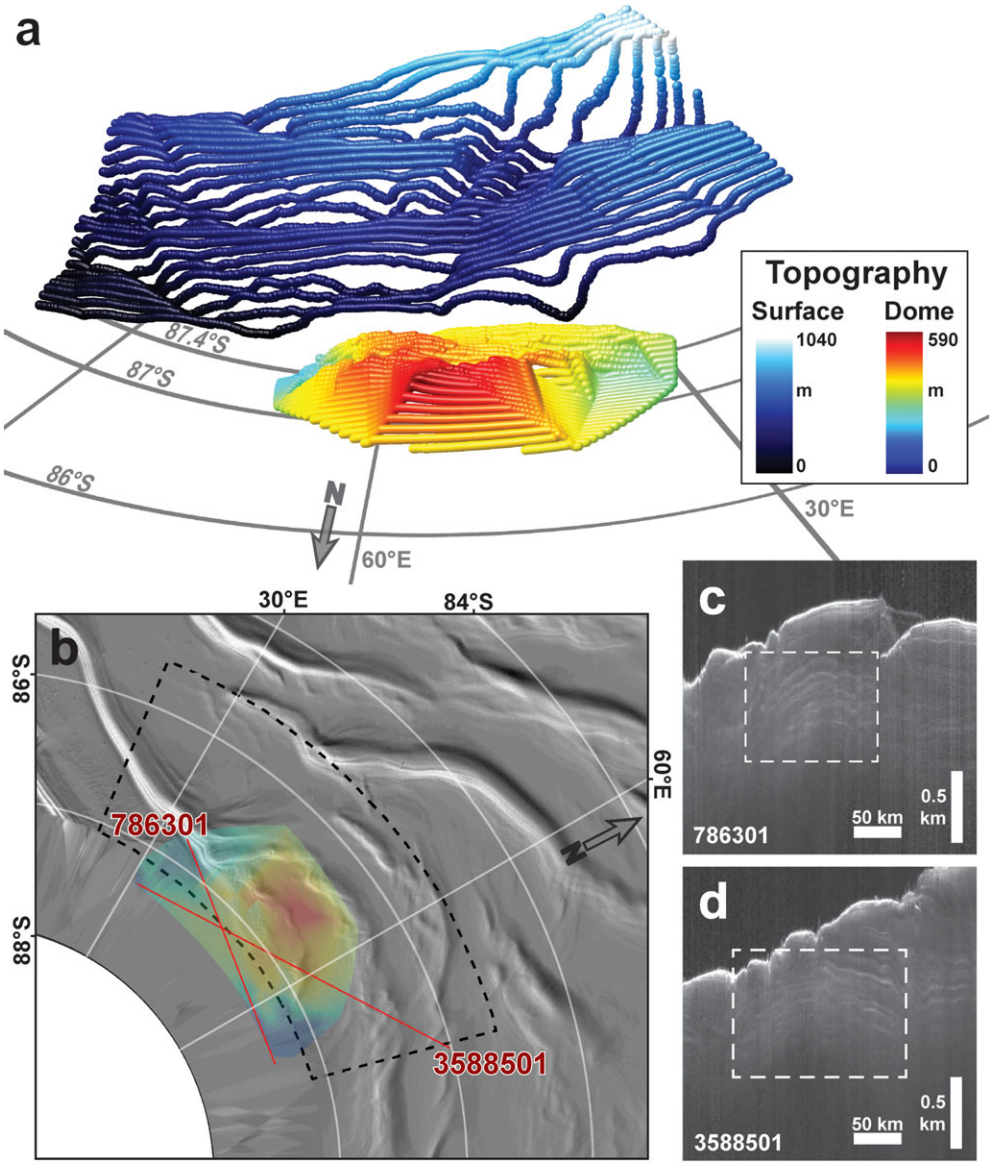

Figure 3. The subsurface elongate dome. (a) A 3-D view of the subsurface dome, interpolated from 24 SHARAD radargrams, offset from the surface for clarity. Surface elevation from MOLA. (b) Aerial view of the subsurface elongate dome (see white box from Figure 1). Black dashed box corresponds to the data shown in Figure 3a. Red lines show the location of Figures 3c and 3d. MOLA hillshade overlain by interpolated dome topography; color scale for the dome topography is the same in Figures 3a and 3b. Close view of the domical cross sections identified within the summed depth-corrected radargram tracks: (c) 786301 and (d) 3588501.

of the cap [*Plaut et al.,* 2007], the elongate dome has an approximate minimum volume of ~2×10^4 km^3, or ~1.25% of the SPLD.

4. Formation of the Elongate Dome

There are several possible formation mechanisms for this large elongate dome, including the presence of thick CO_2 ice layers, deflection of the ice by basal topography or another preexisting structure (i.e., ancient remnant ice cap), or an ice/snow depositional center. Here we assess each potential mode of formation and justify our proposed mechanism.

In the SHARAD data, there is the potential for convex upward features to result from an error in the applied depth correction [*Phillips et al.,* 2011]. Only water ice is assumed for the applied depth correction here. If

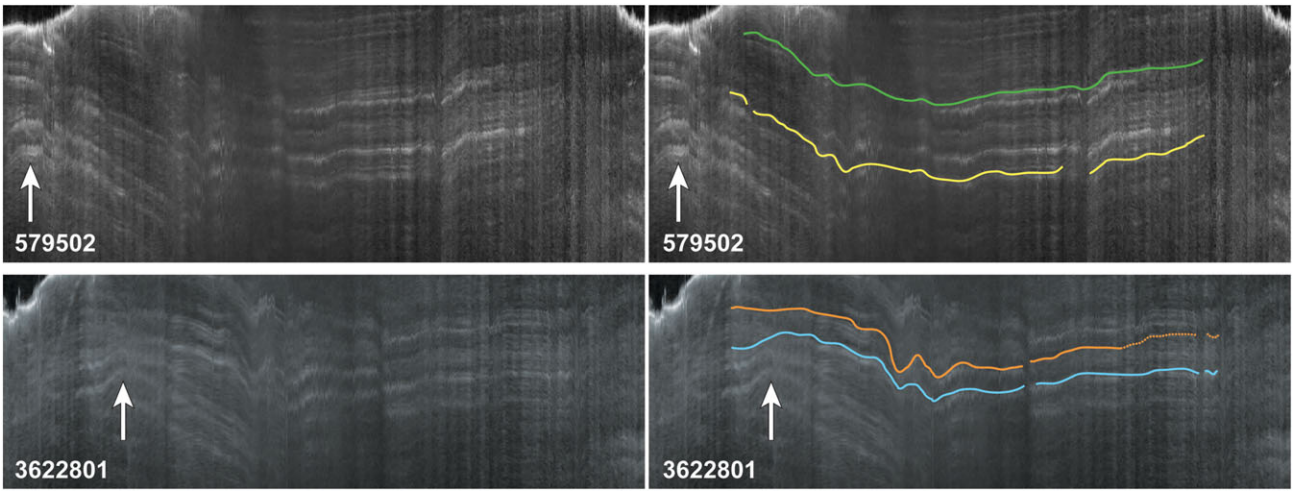

Figure 4. Continuous subsurface interfaces from the elongate dome to the horizontal layer packets. Subsection of depth-corrected SHARAD radargrams 579502 (top row) and 3622801 (bottom row) showing the lack of unconformities. White arrows denote the approximate location of the dome crest centerline, and colored lines trace two separate radar interfaces (which are not the same in these two radargrams); a dotted pattern indicates a lower confidence in the location of the layer position. The 3622801 blue line corresponds to the radar reflector mapped in Figure 3. Images are 360 km across; images are ~940 m (Figure 4, top row) and ~790 m (Figure 4, bottom row) high.

instead there is CO_2 ice above the apparently curved layers, its lower real dielectric constant ($\varepsilon' = 2.1$ [*Simpson et al.,* 1980; *Pettinelli et al.,* 2003]) would create a false convex upward shape. Comparison with maps of the distribution of massive near-subsurface CO_2 ice [*Phillips et al.,* 2011; *Bierson et al.,* 2016] indicates that the elongate dome is not located directly beneath any identified CO_2 deposit. CO_2 ice attenuates the radar signal less than H_2O ice and dust, resulting in increased radar echo strengths for underlying reflectors [*Phillips et al.,* 2011]: there is no enhancement of the SHARAD radar signal below the detected dome (Figure 2). Additionally, the lack of signal enhancement in Mars Advanced Radar for Subsurface and Ionospheric Sounding (MARSIS) radargrams, collected at lower frequencies (e.g., 5 MHz), further confirms the absence of CO_2 ice deposits above the observed SPLD elongate dome (Figure S3).

To further ensure that there is not a CO_2 ice reservoir, the thickness of CO_2 required to deflect the uppermost layers in the observed elongate dome away from the elevation of the surrounding horizontal layers was calculated [*Phillips et al.,* 2011]. Generally, the thickness of CO_2 required to align these uppermost layers horizontally would equal or exceed the amount of material that is physically above them by 50–200 m. Even if the thickness calculations were uncertain within 100 m, a substantial and rapid change in the vertical composition of the SPLD is unlikely. There would also need to be an abrupt horizontal compositional change, from hundreds of meters of CO_2 ice above the observed dome to hundreds of meters of H_2O ice. Owing to the difficulty of this compositional structure, the SPLD elongate dome is interpreted as a physical structure, not an artifact of the data processing.

Basal topography, or remnants of a former ice sheet, may have formed the elongate dome. Displacement of the BFL layer from its expected elevation near a section of the buried Prometheus Basin rim demonstrates that basal topography can affect the position of subsurface layers, while not affecting the surface topography [*Byrne and Ivanov*, 2004]. Prometheus Basin (~875 km in diameter) [*Condit and Soderblom*, 1978] formed prior to the emplacement of the SPLD and has created a predictable change in the basal relief. Approximating the basin rim structure by a circle shows that it continues beneath the SPLD, with its southernmost extent near the geographic south pole (Figure 1). The predicted location of the Prometheus Basin rim and the elevated BFL outcrops [*Byrne and Ivanov*, 2004] do not, however, intersect the region of the elongate dome; the elongate dome is located interior to both of these features.

Plaut et al. [2007] produced a map of the SPLD basal interface using 60 MARSIS orbits. The southern half of the Prometheus Basin rim is vaguely identifiable, where the basal interface of the SPLD near 90°E is topographically lower (~0.5 km) than the rest of the basal interface. Immediately below the elongate dome there is a positive relief feature in the basal topography. However, based on the paucity of distinct MARSIS basal

reflector detections in this region of the SPLD (Figure S3), we interpret this topographic feature to be an interpolated artifact, caused by a single debatable data point [*Plaut et al.,* 2007, their Figure 2]. If the basal interface did increase in elevation below the dome, it should be observed in multiple MARSIS tracks, since other lower-lying basal reflectors are detected elsewhere in the SPLD. This is not observed. Thus, neither MARSIS nor SHARAD data provide clear evidence for the presence of preexisting topography, either basal topography or a remnant buried ice sheet, that may affect the SPLD subsurface layer structure.

The sculpting of the elongate dome through differential erosion can also be ruled out as a formation mechanism due to a lack of observed unconformities in the subsurface layers (Figures 2 and 3). If the high central topography of the ridge crest of the elongate dome was the result of erosion, the layers would end abruptly at the edge of the erosional remnant and lateral unconformities would occur at its edges. Individual layers or layer sequences can be traced across the dome, continuing uninterrupted into the more horizontal layering in the thickest regions of the SPLD (Figure 4). Based on the above discussion, we favor the ice/snow depositional center formation hypothesis for the detected SPLD dome.

5. The SPLD Record of the Past Martian Climate

Prior analysis of SHARAD sounder data of the north polar layered deposits (NPLD) indicates that there was a shift in the location of a north polar snow/ice depocenter early in the cap formation. The infilling of a buried chasma and burial of the elongate dome below Gemina Lingula, and the elevation distribution of other paleosurfaces compared with the current NPLD surface topography provide evidence for these nonuniform depositional patterns [*Putzig et al.,* 2009; *Holt et al.,* 2010]. A similar change in depocenter(s) is plausible for the SPLD.

While the current Martian topography influences the south polar climate [*Richardson and Wilson*, 2002; *Colaprete et al.,* 2005], migration of depocenters in the south polar region is supported by a comparison of the position of the highest point on the SPLD plateau, Australe Mensa, the most recently deposited H_2O (and dust) layer sequence (WRAP) [*Smith et al.,* 2016], and the elongate dome (Figure S4). Australe Mensa is at the highest elevations of the SPLD and thus has experienced the most accumulation. Its center is ~200 km west of the elongate dome and in order to be at higher elevations than the dome today, the Australe Mensa region would have experienced substantially more ice and/or snow deposition. The WRAP is the most recent accumulation of H_2O ice, and the thickest part of this deposit is centered at 81.5°S, 25.5°E (Figure S4). It is offset to the northeast from both the elongate dome and Australe Mensa by ~300 km.

In addition, the south polar accumulation zone has decreased in size between the emplacement of the WRAP and the BFL [*Milkovich and Plaut*, 2008]. This observation demonstrates how the most recent climate in the south polar region has not been stable during the lifetime of the SPLD (7–100 Myr [*Herkenhoff and Plaut*, 2000; *Koutnik et al.,* 2002]). Comparison of the areal extent of the identified layer sequences, IL, PLL, BFL, and WRAP [*Milkovich and Plaut*, 2008; *Smith et al.,* 2016], further emphasizes the changing size of the south polar accumulation zone and oscillations of its center position (Figure S4). This observed concentration of recent deposition between 270°E and 90°E thus further supports the hypothesis that the elongate dome is a former ice/snow depositional center.

Further, the variation in layer thickness across the elongate dome supports the hypothesis that it represents a region of increased deposition; a layer sequence at the peak of the dome is up to 30 m thicker than the same layer in the region of horizontal layering. Water ice mounds or domes are observed elsewhere on Mars, such as within impact craters in the north polar region, and are hypothesized to form from local increases in deposition and decreases in ablation [*Brown et al.,* 2008; *Conway et al.,* 2012; *Brothers and Holt*, 2016]. Formation of an elongated dome in the SPLD by enhanced local accumulation is thus plausible.

The subsurface elongate dome indicates that the SPLD was not deposited as a near-horizontal "layer cake." Instead, the emplacement of the SPLD involved uneven deposition of ice and dust, with local depocenters accumulating relatively more material than other regions. The size and vertical extent of the elongate dome suggests a relatively long-lived depositional region that would have been controlled by the climate. The fact that the uppermost and lowermost layer packets (BFL and IL) have approximately the same areal extent [*Milkovich and Plaut*, 2008] (Figure S4), which differs from the PLL sequence and the WRAP, suggests that the IL does not have to be an erosional remnant of the earliest SPLD materials or another ancient ice

sheet. Rather, the IL may represent the maximum depositional extent of the fledgling SPLD when deposition was more similar to today.

After an erosional hiatus, the larger areal extent and sequence thickness of the PLL means it would have formed during a period of higher accumulation rates; increased accumulation is associated with periods of minimal polar insolation and obliquity variations over the last 10 Myr [*Levrard et al.,* 2007]. The presence of SPLD materials within the craters Elim and Katoomba (43.6 km, 80.17°S, 96.80°E, and 51.2 km, 79.01°S, 127.81°E, in diameter, respectively) hint that the SPLD, specifically the PLL layer sequence that corresponds to these intracrater materials, may have been modestly more extensive in the recent past [*Byrne and Ivanov*, 2004; *Rodriguez et al.,* 2015]. The BFL sequence was subsequently deposited during a period of time when the zone of accumulation decreased in areal extent. Lastly, the WRAP was deposited, offset from the SPLD center and covering an even smaller area than the BFL. This smaller extent indicates a further decrease in the zone of accumulation in the south polar region of Mars.

6. Conclusions

The detection of non-horizontal SHARAD radar echoes that form an elongate dome beneath the SPLD surface, coupled with the gradual decrease in the area covered by the zone of accumulation, displays the evolution of the south polar climate over the last >100 Myr. The elongate dome formed during a period of enhanced local deposition within the SPLD. Comparisons of the areal extent of specific polar units (IL, PLL, BFL, and WRAP) with the location of the subsurface dome reveal the oscillatory (in extent and center location) behavior of the ice/snow depocenter in the south polar region of Mars.

Acknowledgments
We wish to thank the two anonymous reviewers for their helpful comments and suggestions. The SHARAD instrument was provided to NASA's Mars Reconnaissance Orbiter (MRO) mission by the Italian Space Agency (ASI), and its operations are led by the DIET Department, University of Rome "La Sapienza" under an ASI contract. This work was funded under JPL contracts to the MRO-SHARAD science team. The authors thank the MRO mission team and the SHARAD instrument team for their efforts in acquiring the radar sounder data set. All data supporting these results can be found in the supporting information and NASA's Planetary Data System.

References

Bibring, J.-P., et al. (2004), Perennial water ice identified in the south polar cap of Mars, *Nature*, *428*, 627–630, doi:10.1038/nature02461.
Bierson, C. J., R. J. Phillips, I. B. Smith, S. E. Wood, N. E. Putzig, D. Nunes, and S. Byrne (2016), Stratigraphy and evolution of the buried CO2 deposits in the Martian south polar cap, *Geophys. Res. Lett.*, *43*, 4172–4179, doi:10.1002/2016GL068457.
Brothers, C. T., and J. W. Holt (2016), Three-dimensional structure and origin of a 1.8 km thick ice dome within Korolev Crater, Mars, *Geophys. Res. Lett.*, *43*, 1443–1449, doi:10.1002/2015GL066440.
Brown, A. J., S. Byrne, L. L. Tornabene, and T. Roush (2008), Louth crater: Evolution of a layered water ice mound, *Icarus*, *196*, 433–445, doi:10.1016/j.icarus.2007.11.023.
Byrne, S., and A. B. Ivanov (2004), Internal structure of the Martian south polar layered deposits, *J. Geophys. Res.*, *109*, E11001, doi:10.1029/2004JE002267.
Campbell, B. A., G. A. Morgan, N. E. Putzig, J. W. Holt, and R. J. Phillips (2014), Properties of the Mars polar layered deposits from radar sounding, *Intl. Conf. Mars 8*, abstract 12350.
Campbell, B. A., G. A. Morgan, N. E. Putzig, J. L. Whitten, J. W. Holt, and R. J. Phillips (2015), Enhanced radar visualization of structure in the south polar deposits of Mars, *Lunar Planet. Sci. Conf.* 46, abstract 2366.
Christian, S., J. W. Holt, S. Byrne, and K. E. Fishbaugh (2013), Integrating radar stratigraphy with high resolution visible stratigraphy of the north polar layered deposits, Mars, *Icarus*, *226*, 1241–1251, doi:10.1016/j.icarus.2013.07.003.
Colaprete, A., J. R. Barnes, R. M. Haberle, J. L. Hollingsworth, H. H. Kieffer, and T. N. Titus (2005), Albedo of the south pole on Mars determined by topographic forcing of atmospheric dynamics, *Nature*, *435*, 184–188, doi:10.1038/nature03561.
Condit, C. D., and L. A. Soderblom (1978), Geologic map of the Mare Australe area of Mars, USGS Misc. Invest. Ser. Map, I-1076.
Conway, S. J., N. Hovius, T. Barnie, J. Besserer, S. Le Mouélic, R. Orosei, and N. A. Read (2012), Climate-driven deposition of water ice and the formation of mounds in craters in Mars' north polar region, *Icarus*, *220*, 174–193, doi:10.1016/j.icarus.2012.04.021.
Grima, C., W. Kofman, J. Mouginot, R. J. Phillips, A. Hérique, D. Biccari, R. Seu, and M. Cutigni (2009), North polar deposits of Mars: Extreme purity of the water ice, *Geophys. Res. Lett.*, *36*, L03203, doi:10.1029/2008GL036326.
Herkenhoff, K. E., and B. C. Murray (1990), Color and albedo of the South Polar Layered Deposits on Mars, *J. Geophys. Res.*, *95*, 1343–1358, doi:10.1029/JB095iB02p01343.
Herkenhoff, K. E., and J. J. Plaut (2000), Surface ages and resurfacing rates of the Polar Layered Deposits on Mars, *Icarus*, *144*, 243–253, doi:10.1006/icar.1999.6287.
Holt, J. W., K. E. Fishbaugh, S. Byrne, S. Christian, K. Tanaka, P. S. Russell, K. E. Herkenhoff, A. Safaeinili, N. E. Putzig, and R. J. Phillips (2010), The construction of Chasma Boreale on Mars, *Nature*, *465*, 446–449, doi:10.1038/nature09050.
Howard, A. D., J. A. Cutts, and K. R. Blasius (1982), Stratigraphic relationships within Martian polar cap deposits, *Icarus*, *50*, 161–215, doi:10.1016/0019-1035(82)90123-3.
Johari, G. P. (1976), The dielectric properties of H_2O and D_2O ice Ih at MHz frequencies, *J. Chem. Phys.*, *64*, 3998–4005, doi:10.1063/1.432033.
Koutnik, M., S. Byrne, and B. Murray (2002), South Polar Layered Deposits of Mars: The cratering record, *J. Geophys. Res.*, *107*(E11), 5100, doi:10.1029/2001JE001805.
Levrard, B., F. Forget, F. Montmessin, and J. Laskar (2007), Recent formation and evolution of northern Martian polar layered deposits as inferred from a global climate model, *J. Geophys. Res.*, *112*, E06012, doi:10.1029/2006JE002772.
Milkovich, S. M., and J. J. Plaut (2008), Martian South Polar Layered Deposit stratigraphy and implications for accumulation history, *J. Geophys. Res.*, *113*, E06007, doi:10.1029/2007JE002987.
Milkovich, S. M., J. J. Plaut, A. Safaeinili, G. Picardi, R. Seu, and R. J. Phillips (2009), Stratigraphy of the Promethei Lingula, south polar layered deposits, Mars, in radar and imaging datasets, *J. Geophys. Res.*, *114,* E03002, doi:10.1029/2008JE003162.
Murray, B. C., L. A. Soderblom, J. A. Cutts, R. P. Sharp, D. J. Milton, and R. B. Leighton (1972), Geological framework of the south polar region of Mars, *Icarus*, *17*, 328–345, doi:10.1016/0019-1035(72)90004-8.

Murray, B. C., W. R. Ward, and S. C. Yeung (1973), Periodic insolation variations on Mars, *Science*, *180*, 638–640, doi:10.1126/science.180.4086.638.

Nye, J. F., W. B. Durham, P. M. Schenk, and J. M. Moore (2000), The instability of a south polar cap on Mars composed of carbon dioxide, *Icarus*, *144*, 449–455, doi:10.1006/icar.1999.6306.

Pettinelli, E., G. Vannaroni, A. Cereti, F. Paolucci, G. Della Monica, M. Storini, and F. Bella (2003), Frequency and time domain permittivity measurements on solid CO_2 and solid CO_2-soil mixtures as Martian soil simulants, *J. Geophys. Res.*, *108*(E4), 8029, doi:10.1029/2002JE001869.

Phillips, R. J., et al. (2011), Massive CO2 ice deposits sequestered in the South Polar Layered Deposits of Mars, *Science*, *332*, 838–841, doi:10.1126/science.1203091.

Plaut, J. J., et al. (2007), Subsurface radar sounding of the South Polar Layered Deposits of Mars, *Science*, *316*, 92–95, doi:10.1126/science.1139672.

Putzig, N. E., R. J. Phillips, B. A. Campbell, J. W. Holt, J. J. Plaut, L. M. Carter, A. F. Egan, F. Bernardini, A. Safaeinili, and R. Seu (2009), Subsurface structure of Planum Boreum from Mars Reconnaissance Orbiter Shallow Radar soundings, *Icarus*, *204*, 443–457, doi:10.1016/j.icarus.2009.07.034.

Richardson, M. I., and R. Wilson (2002), A topographically forced asymmetry in the martian circulation and climate, *Nature*, *416*, 298–301, doi:10.1038/416298a.

Rodriguez, J. A. P., et al. (2015), New insights into the Late Amazonian zonal shrinkage of the martian south polar plateau, *Icarus*, *248*, 407–411, doi:10.1016/j.icarus.2014.08.047.

Seu, R., D. Biccardi, R. Orosei, L. V. Lorenzoni, R. J. Phillips, L. Marinangeli, G. Picardi, A. Masdea, and E. Zampolini (2004), SHARAD: The MRO 2005 shallow radar, *Planet. Space Sci.*, *52*, 157–166, doi:10.1016/j.pss.2003.08.024.

Seu, R., et al. (2007), SHARAD sounding radar on the Mars Reconnaissance Orbiter, *J. Geophys. Res.*, *112*, E05S05, doi:10.1029/2006JE002745.

Simpson, R. A., B. C. Fair, and H. T. Howard (1980), Microwave properties of solid CO_2, *J. Geophys. Res.*, *85*, 5481–5484, doi:10.1029/JB085iB10p05481.

Smith, D. E., et al. (2001), Mars Orbiter Laser Altimeter: Experiment summary after the first year of global mapping of Mars, *J. Geophys. Res.*, *106*, 23,689–23,722, doi:10.1029/2000JE001364.

Smith, I. B., N. E. Putzig, J. W. Holt, and R. J. Phillips (2016), An ice age recorded in the polar deposits on Mars, *Science*, *352*, 1075–1078, doi:10.1126/science.aad6968.

Thomas, P., S. Squires, K. Herkenhoff, A. Howard, and B. Murray (1992), Polar deposits on Mars, in *Mars*, pp. 767–795, Univ. Arizona Press, Tucson.

Titus, T. N., H. H. Kieffer, and P. R. Christensen (2003), Exposed water ice discovered near the South Pole of Mars, *Science*, *299*, 1048–1051, doi:10.1126/science.1080497.

Toon, O. B., J. B. Pllack, W. Ward, J. A. Burns, and K. Bilski (1980), The astronomical theory of climatic change on Mars, *Icarus*, *44*, 552–607, doi:10.1016/0019-1035(80)90130-X.

Zuber, M. T., R. J. Phillips, J. C. Andrews-Hanna, S. W. Asmar, A. S. Konopliv, F. G. Lemoine, J. J. Plaut, D. E. Smith, and S. E. Smrekar (2007), Density of Mars' South Polar Layered Deposits, *Science*, *317*, 1718–1719, doi:10.1126/science.1146995.